Chapter 7
Optimizing NVH Performance in Electric Vehicles Through Enhanced Modal Parameter Estimation Techniques

Mahmoud Elkafafy and Marc Brughmans

Abstract When analyzing the NVH characteristics of an electric vehicle (EV) it is important to consider the effect of the battery on the dynamic characteristics of the body. When a negative impact on the body stiffness performance is noticed, body design improvements are needed to counteract the battery structural influence. A hybrid modeling environment in which a test-based battery subsystem is coupled to an FE-based body representation is ideal for this design optimization study. Frequency based substructuring techniques are typically used in such hybrid modeling environments. Due to the large mumber of interfaces DoFs between body and battery, the mumber of involved FRFs in the coupling is high ($>$ 6000 FRFs) and this poses huge challenges to the quality of the matrix inversion in the coupling operator. In such a large FRF data set the inherent observed noise and small phase inconsistencies between the FRFs can play an important role in the matrix condition of the inversion. A smoothed approximation of the FRF is needed to provide a more stable coupling condition In this paper, the MLMM modal parameter estimation method is used to achieve this smoothed approximation of the FRFs by identifying a high-quality modal model of the battery. One challenge here is that the FRFs in the different directions are different in magnitude which could lead to a poor fit quality for those FRFs that have a lower magnitude (e.g., the implane-directions' FRFs). A balancing approach will be introduced and applied to the FRFs matrix to ensure that all FRFs will equally be weighted during the modal parameter estimation process. Another challenge here is that the battery pack is coupled to the body over a large mounting area involving a large number of coupling points. This implies that a large number of FRFs are involved in the modal parameter estimation process which induces a very challenging optimization task in the MLMM method to curve fit both the global and local dynamic responses at the same time. A 2-steps workflow that delivers a full modal model of the battery, which includes all the excitation DoFs (i.e., all the coupling DoFs), starting form a limited number of FRFs matrix 's columns (i.e., a subset of the excitation DoFs) in an efficient way will be presented and validated. The proof-of-concept of the developed method is first demonstrated on a large FRF set obtained by simulation. In a second step the method has been applied on a large set of measured FRFs.

Keywords Electric vehicle · NVH · MLMM · Modal · Substucturing

Introduction

The shift of the automotive industry to Electric Vehicles (EV) brought new challenges to the development of vehicle body. The introduction of the battery pack has deeply changed the structural and dynamic behavior of the vehicle. The body design is reviewed, and structural improvements are proposed to accommodate the heavy battery structure. In this development process an accurate simulation model is needed for both body and battery stuctures. The simulation of body structures has been around for a long time, so a lot of experience is available to build an accurate model. Less experience is around for building an accurate battery structural model. When building a full FE based body-battery system model there is a danger that the quality of the simulation results is jeopardized by a lower quality FE representation of the battery. Directions for body design improvements may be biased by a wrong simulated battery behavior. Therefore, in the cases that the battery design is fixed, and hardware is available, it would be a much better option for the body designer to represent the battery with an accurate test-based modal model.

A first step in building a test-based modal model is to perform FRFs measurements on the battery at all points that interface with the body structure. These measured FRFs can directly be used in Frequency Based Substructuring (FBS)

Mahmoud Elkafafy · Marc Brughmans
Siemens Industries Software NV, Interleuvenlaan 68, 3001 Leuven, Belgium
e-mail: mahmoud.el-kafafy@siemens.com

Brandon Dilworth et al. (eds.), *Topics in Modal Analysis & Parameter Identification II, Vol. 10*, Conference Proceedings of the Society for Experimental Mechanics Series, https://doi.org/10.13052/97887-438-0155-9_7

techniques to build a full vehicle model. However, due to the large number of interfaces degrees of freedom (DoFs) between body and battery, the number of involved FRFs in the coupling is high (> 6000 FRFs) and this poses high challenges to the quality of the matrix inversion in the coupling operator. In such a large FRF data set the inherent observed noise and small phase inconsistencies between the FRFs can play an important role in the matrix condition of the inversion [1].

In this paper, we propose a method for realizing a more stable coupling condition that is based on high quality modal model that provides an accurate smoothed approximation of the measured FRFs. Several roadblocks have to be resolved to obtain such a modal model in an accurate and efficient way giving the fact that a large number of potentially magnitude-unbalanced FRFs need to be processed. The next sections will present these challenges and discuss the developed solutions from a theoretical point of view. Afterwards, the developed solutions are applied in a CAE modeling environment to validate the workflow and provide a proof of concept. Finally, the new developed techniques are demonstrated using frequency response functions (FRFs) measured on a battery structure provided by Hyundai Motor Company (HMC).

Background and Proposed Workflow

In this section, we introduce the proposed workflow for estimating high-quality modal model of a sub-component to be coupled (e.g., the battery pack) in an efficient manner. Given that the raw FRFs matrix to be processed to reach the intended modal model involves a large number of functions (78 rows × 78 columns at each frequency line) and those functions could potentially be magnitude-imbalanced, the workflow aims to address two key aspects: 1) ensuring reasonably accurate modal synthesis for all FRFs, regardless of their magnitude level, and 2) executing the modal estimation process in a time-efficient manner. The different blocks of the proposed workflow are illustrated in Fig. 1. As shown in the figure, the workflow consists of two main steps: 1) estimating a reduced-size, in terms of reference DoFs , modal model, and 2) expanding the reduced-size modal model to the full original-size FRFs matrix.

To estimate a reduced-size modal model, a selection of a few columns (e.g., $N_{i_{Red}} = 4$, with $N_{i_{Red}}$ the reduced selected number of columns) from the full-size FRFs matrix must be made. After selecting the recluced number of columns, the first step in the workflow, estimating reduced-size participation factor vectors, consists of three main sub-steps. In the first substep, a magnitude-based balancing approach is applied to the rechuced FRFs matrix to equalize the different FRFs in terms of magnitude. In the second sub-step, the modal parameters of the component under test (CUT) are estimated in the frequency band of interest by applying the well-known Polymax and MLMM (Maximum Likelihood estimation of a Modal Model) estimators [2, 3] to the balanced reduced-size FRFs matrix. Finally, in the third sub-step, the estimated mode shape vectors, participation factor vectors, and elements of the lower and upper residual terms matrices are rescaled to make them

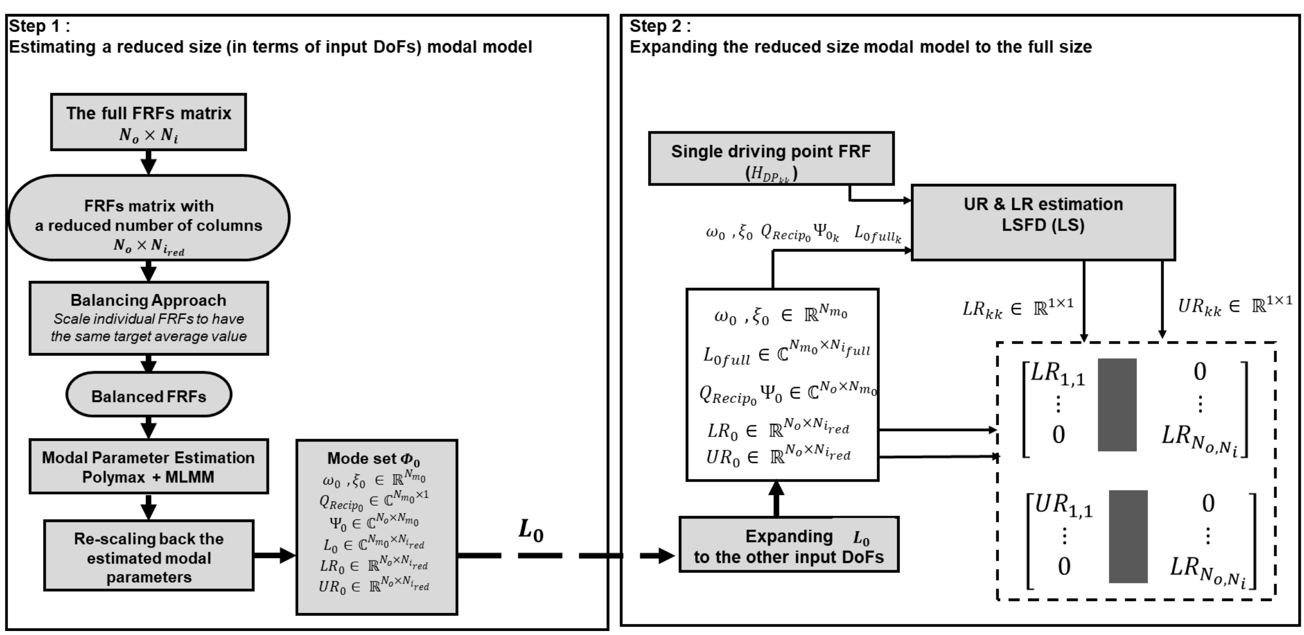

Fig. 1 The workflow of the proposed enhanced modal parameter estimation approach

consistent with the original magnitude levels of the processed FRFs. Once the reduced-size modal model is estimated, a full-size modal model is retrieved by extending the estimated participation factor vectors, the lower residual matrix, and the upper residual matrix in the second step of the proposed workflow. In the following sub-sections, futher details and background information on each sub-step are provided.

FRFs Magnitude-Based Balancing Approach

In curve-fitting techniques, such as linear least-squares (LLS)-based or nonlinear least-squares (NLS)-based fitters, there is a risk that the fitting process becomes biased toward subsets of the input data matix with relatively higher magnitudes, thereby neglecting the lower-magnitude subsets. In such a scenario, the regression model disproportionately favors certain data points, often those with higher values or greater variance, while underweighting or 'forgetting' data points with lower values. Since these are essentially least-squares-based techniques, advanced frequency-domain modal parameter estimators, such as Polymax, MLMM, and others [2–4], could face this issue if the primary imput data matrix (e.g., an FRFs matrix) is imbalanced in terms of the magnitude levels of its individual entries. This imbalance in the magnitude levels of the measured response functions could be due to several factors: differences in the stiffness of the component under test (CUT) across vanious directions or paths, the inclusion of both translational and rotational responses in the measured DoFs (e.g., translational and rotational accelerations), or the involvement of quantities with mixed units in the measured FRFs matrix (e.g., vibroacoustic modal test where structural and acoustic FRFs are acquired).

In the context of modal model-based structural coupling (or component mode substructuring CMS), it is crucial to ensure that all the FRFs at the coupling DoFs, specifically those involving co-located measurements of responses and forces, are accurately represented by the identified modal model. In an electric vehicle battery-like structure, the response magnitudes in the x and y (i.e, longitudinal and lateral) directions are relatively lower than those in the z (i.e., vertical) direction due to the battery's geometry. This results in lower-magnitude FRFs in the x and y directions and higher-magnitude FRFs in the z-direction. Figure 2 shows typical driving point FRFs extracted from an EV battery's finite element model (FEM), where the difference in magnitude across the x, y, and z directions is clearly visible. Performing a modal parameters estimation using an FRFs matrix that contains such different in magnitude functions could end with biased results, as not all FRFs in the input matrix would be appropriately considered. The FRFs in x and y-directions may be underweighted during the modal fitting process compared to those in the z-direction, leading to enroneous modal synthesis for those FRFs. This would certainly result in inaccurate body-to-battery coupling result. A similar issue of unbalanced FRFs can occur on the car body side. For example, a DoF measured on the roof of the car body, which is an important DoF for visualizing global modes, will have a significantly higher amplitude than a DoF measured on the driver's seat rail or a DoF at the body-to-battery connection points, which are used for target settings and structural coupling, respectively. This imbalance could mislead the modal estimation technique, causing it to focus on the higher-magnitude DoFs while neglecting the ones that are more critical for analysis (i.e., the coupling and target settings DoFs).

In this work, a magnitude-based balancing approach will be implemented to ensure that all individual FRFs will appropriately be considered by the Polymax and MLMM modal parameter estimators during the modal parameter estimation step. The implemented balancing approach aims to scale all individual FRFs so that they have the same target average value (e.g., mean, median, RMS value) equals to 1 over the selected fiequency band of interest. This is achieved by scaling each function in the FRFs matrix with its calculated 'selected' central tendency criterion Γ_{ot} with $o = 1, 2, \ldots, N_o$ and $i = 1, 2, \ldots, N_t$, where N_o and N_l are the mumber of outputs (responses DoFs) and inputs (excitation DoFs) respectively. The effect of this scaling mechanism is shown in Fig. 3 where the unbalanced FRFs (cf. Fig. 2) are now getting closer to each other in terms of magnitude level. Scaling the magnitude of the raw FRFs will consequently influence the magnitudes of the estimated mode

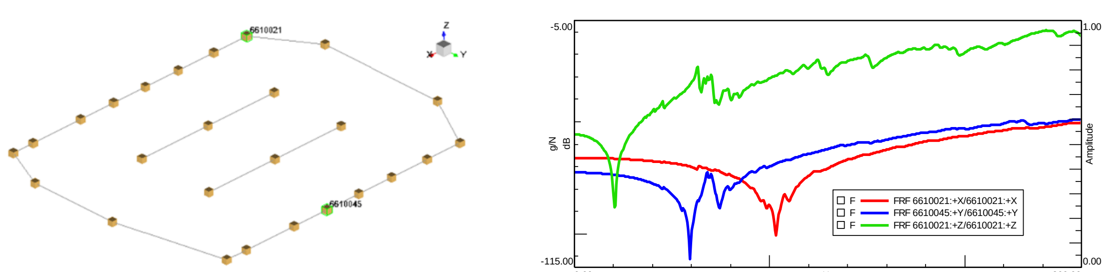

Fig. 2 Right: typical driving point FRFs in different directions extracted from an EV battery's FEM. Left: the geometry of the battery of an EV highlighting the selected driving point locations

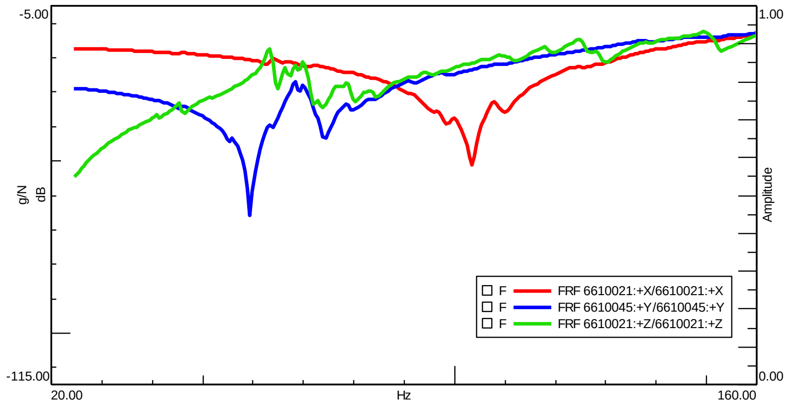

Fig. 3 The effect of the balancing approach on the magnitude level of originally unbalanced FRFs (cf. Fig. 2)

shapes, participation factor vectors, and the lower and upper residual terms (cf, equation (1)). This means that the estimated modal vectors (i.e, mode shapes and participation factors vectors), along with the residual terms, will need to be rescaled back to their expected correct magnitude levels that are consistent with the magnitude levels of the original raw FRFs.

To achieve this, the scaling coefficient Γ_{oi} used to scale an individual FRF H_{oi} needs to be split into two coefficients $\Gamma_{ol} = \alpha_o \beta_i$, with $o = 1, 2, \ldots, N_o$ and $i = 1, 2, \ldots, N_i$. The α_o's coefficients will be used to rescale the mode shape elements, while the β_i's coefficient will be used to rescale the participation factor vectors for each identified mode. The Γ_{oi} coefficients will be used to rescale the entries of the lower and upper residual matrices. Expressing the relationship $\Gamma_{oi} = \alpha_o \beta_l$ in a set of linear equations, one can determine the α_0 and the β_1 coefficients by solving a linear least-squares problem considering the constraint for preserving the FRFs reciprocity property if needed.

Modal Parameter Estimation: Polymax & MLMM Estimators

In this step, the Simcenter MLMM modal parameter estimator [3] will be applied to the balanced FRFs matrix to estimate a modal model that can represent the measured FRFs with a reasonable accuracy within a specified frequency band. To expedite the modal estimation step, the FRFs matnix with the full set of columns (in our case this corresponds to $N_i = 78$) will not be used Instead, a significantly reduced FRFs matrix with fewer columns (e.g., $N_{i_{Red}} = 4$) will be provided as input data to the MLMM estimator. There is no specific theory to guide users in selecting the rechuced number of references DoFs (in terms of quantity and location). However, a rule of thumb from domain knowledge suggests that the selected reference DoFs should ensure excitation in all directions (vertical, lateral, and longitudinal) and should not be concentrated on one side of the component under test (CUT).

The modal model given by Eq. (1) decomposes the frequency response functions (FRFs) matrix of a dynamical system $\boldsymbol{H}(s_k) \in \mathbb{C}^{N_0 \times N_i \times N_f}$, with $s_k = j\omega_k$ the complex fiequency at frequency line k where $k = 1, 2, \ldots, N_f$, as a linear sum of the different N_m vibroacoustic modes represented by their corresponding modal parameters $\psi_r \in \mathbb{C}_0^{N_o \times 1}$ the r^{th} mode shape column vector, $\lambda_r \in \mathbb{C}$ the r^{th} pole from which the natural fiequency and the damping ratio are deduced, and $L_r \in \mathbb{C}^{1 \times N_t}$ the r^{th} participation factor row vector.

$$\boldsymbol{H}(s_k) = \left(\sum_{r=1}^{N_m} \left(\frac{\psi_r L_r}{s_k - \lambda_r} + \frac{\psi_r^* L_r^*}{s_k - \lambda_r^*} \right) \right) + \frac{\boldsymbol{LR}}{s_k^2} + \boldsymbol{UR} \tag{1}$$

In Eq. (1), (.)* stands for the complex conjugate of a complex-valued parameter, $\boldsymbol{LR} \in \mathbb{R}^{N_0 \times N_l}$ and $\boldsymbol{UR} \in \mathbb{R}^{N_0 \times N_l}$ are the lower and upper residual terms respectively that are used to model the influence of the modes that are located respectively below and above the fiequency range of interest considering a displacement over force FRF format. The upper residual term (***UR***), also called the stiffness residual, is essentially a constant that models the asymptotic contribution of modes located at frequencies far above the frequency band of interest. This term, particularly its diagonal elements, is crucial for accurately modeling the dynamics of a coupling DoF (i.e, a driving point DoF), as it compensates for the local stiffless contribution that is not captured by the global modes within the frequency band of interest. The lower residual, also known as the mass residual, models the asymptotic contribution of modes located far below the fiequency band of interest. This contribution decays with the square of the fiequency.

The MLMM modal parameter estimation method [3] is a multivariable (i.e., MIMO) frequency-domain method that uses the modal model (1) as a parametric model to represent the measured FRFs over a chosen frequency band. The MLMM method differs from the existing modal parameter estimation methods in the sense that it directly optimizes the modal model, represented by equation (1), rather than optimizing a high order rational fiaction polynomial-based model and reducing it in a subsequent step to a modal model. Such model reduction would most likely lead to a degradation in the quality of the fit between the measured data and the final estimated modal model In the MLMM method, the Levenberg-Marquardt optimization algorithm tunes the parameters of the modal model (1) to minimize a quadratic-like cost function (i.e., sum of the squared enror between the true data and the data synthesized by the modal model) so that a best match between the modal model (1) and the measurements is obtained. In the optimization process, the user has also the option to apply some physically motivated constraints to the modal model, e.g. FRFs reciprocity constraint, real mode shapes constraint, and the negative mass sensitivity (NMS) characteristic constraint. The inputs needed from the user in the MLMM step are the maximum number of iterations for the iterative Levenberg-Marquardt optimization process, the choice of including/excluding the lower and upper residual terms, and if constraints are to be applied to the modal model. In this work, the MLMM estimator will be applied to estimate a constained modal model, where FRFs reciprocity, real mode shapes, and NMS constraints are imposed on the identified modal model. The FRFs reciprocity constraint is crucial for the subsequent expansion step, where the modal model will be expanded to match the full size of the original FRFs matnix (i.e., from $N_{i_{Red}} = 4$ to $N_i = 78$). The NMS and real mode shape constraints are imposed not only to preserve the physicalness of the identified modes and facilitate mode shape visualization but also to ensure that the identified mode set is exportable to Simcenter Nastran, where the battery-to-body coupling activities will be carried out.

Since MLMM runs a nonlinear optimization process, it requires initial values for the system poles $\lambda_r \in \mathbb{C}$ and the participation factors $L_r \in \mathbb{C}^{1\times N_l}$ for each identified mode within the flequency band of interest. The well-known linear least-squares-based modal estimator Polymax [2] will be used to generator these initial values for the MLMM estimator. In a nutshell, the Polymax estimator requires FRFs as primary data and identifies, by fitting those FRFs, the numerator and denominator matrix polynomial coefficients of a right matrix fraction description (RMFD) polynomial transfer function model defined with a model order p set for both the numerator and the denominator polynomials. Those coefficients are identified by solving a linear least squares problem with a cost function given as the squares of the (lineanized) fit enror between the measured FRFs and the RMFD model. Once the denominator matrix polynomial coefficients are estimated, the eigenvalues λ_r and the modal participation factors L_r are calculated by computing the eigenvalue decomposition of their companion matrix. An important user choice is the polynomial model order p, which is related to $n = 2N_m$, the number of poles in the system as: $n = pN_i$. Rather than fixing the model order a priori, a whole range of models with increasing model orders (up to a maximum model order p) is calculated. The poles conesponding to a certain model order are compared to the poles of a one-order-lower model If their differences in terms of frequency, damping, and eigenvectors are within pre-set limits, the pole is labelled as a stable one. The spurious numerical poles will not stabilize at all during this process and can be sorted out of the set of poles more easily, e.g., by interpreting so-called stabilization diagrams. A stabilization diagram is a 2D plot showing all poles from all identified models, sorted according to frequency values (x-axis) and model order (y-axis), cf. Figure 16 for instance. In such diagram, the stable poles will also appear as clusters and a representative of each cluster can be selected for the final mode set. One big advantage of the Polymax estimator is that it delivers a very clear stabilization diagram which helps the user to easily select the physical modes and to set up the proper model size of the analyzed system. Altematively, the constructed stabilization diagram can be automatically interpreted instead [5] where the mumber of stable pole clusters determines the model order and a pole estimate (and the corresponding participation factors) for each cluster is calculated. The inputs needed from the user in the Polymax step are the maximum polynomial order p and the fiequency band of interest $[f_{\min}, f_{\max}]$.

As mentioned earlier, the balanced FRFs-based estimated modal parameters (mode shape vectors, participation factor vectors, lower residuals, and upper residuals) need to be rescaled to make them consistent with the magnitude level of the original imbalanced FRFs. The estimated scaling coefficients α_o's and the β_l's (cf. the FRFs balancing section) will be used to do this rescaling process.

Modal Model Expansion

After estimating a reduced-size (in terms of the number of reference DoFs) reciprocal modal model using the Polymax and MLMM modal estimators, the estimated participation factor vectors, along with the lower and upper residual matrices, will be expanded to the fill number of reference DoFs (i.e., from $N_{i_{Red}} = 4$ to $N_i = 78$). A reciprocal modal model means that the lower and upper residual matrices are symmetric, and for each identified mode, the mode shape coefficient at an imput DoF is proportional to the participation factor at that imput DoF, up to a scaling factor (i.e, the reciprocal scaling factor). When the reciprocity constraint is applied during the MLMM iterations, the MLMM estimator produces the following modal model:

$$\boldsymbol{H}_{Red}\left(s_k\right)=\left(\sum_{r=1}^{N_m}\left(\frac{Q_r\phi_r L_{Red_r}}{s_k-\lambda_r}+\frac{Q_r^*\phi_r^* L_{Red_r^*}^*}{s_k-\lambda_r^*}\right)\right)+\frac{\boldsymbol{LR}_{Rec}}{s_k^2}+\boldsymbol{UR}_{Rec} \tag{2}$$

with, for the r^{th} mode, $Q_T \in \mathbb{C}$ the reciprocal scaling factor, $\phi_r \in \mathbb{C}^{N_o\times 1}$ the mode shapes vector in which the shape coefficient conresponds to an input DoF considered to be proportional to the participation factor at that input DoF up to a scale factor $Q_r, L_{Red_i} \in \mathbb{C}^{1\times N_{i_{Red}}}$ the reduced size participation factors vector, $\boldsymbol{LR}_{Rec} \in S^{N_0\times N_{i_{Red}}}$ and $\boldsymbol{UR}_{\text{Rec}} \in S^{N_0\times N_{i_{Red}}}$ the reduced size symmetric lower and upper residual matrices. In case the real shape and the negative mass sensitivity constraints are also imposed, the product $Q_r\phi_r L_{Red_r}$ becomes an imaginary-valued matrix, where the element conresponding to a driving point DoF is imposed to be a negative imaginary value. Having identified the reciprocal modal model (2) with the reciprocal scaling factors Q_r, the expanded participation factors vector $L_r \in \mathbb{C}^{1\times N_i}$ for each identified mode r is simply the transpose of the corresponding mode shapes vector:

$$L_r = \phi_r^T \in \mathbb{C}^{1\times N_0} \tag{3}$$

For the lower and upper residual terms (***LR*** & ***UR***), it is not feasible to fully expand those matrices to obtain all $N_o \times N_o$ elements, as was done for the modal kernel term (also known as the global flexable modes term). However, neglecting these terms can lead to significant errors in modal synthesis, especially if lower and/or higher-fiequency modes are truncated. This issue is particularly critical for a driving point degree of freedom (DoF). The global flexible modes and the higher-fiequency truncated modes, represented by the upper residual term (***UR***), both contribute to the local flexability at a driving point degree of freedom (DoF). The more significant the higher-fiequency truncated modes are, the more critical the ***UR*** contribution becomes to local flexability. Consequently, the diagonal elements of the upper residual term (***UR***) are essential for achieving an accurate modal synthesis of a frequency response function (FRF) of a driving point. Higher-frequency truncated modes contribute more significantly to local flexability, i.e., the diagonal elements of the upper residual term (***UR***), rather than to global flexibility, which is primanily captured by the contributions of global flexible modes. Therefore, a reasonable approximative solution for expanding the ***UR*** matrix is to focus only on the diagonal elements. This approach would provide an accurate modeling of local stiffness for the driving point degrees of freedom (DoFs), which are essentially the coupling DoFs between the car body and the battery structure. For the lower residual (***LR***) matrix, the same scheme used for the upper residual (***UR***) matrix will be followed, focusing on extending only the diagonal elements. The contribution of the ***LR*** matrix to the overall dynamics of the component under test is found to be minor compared to that of the ***UR*** matrix. This is because the analyzed frequency band typically includes the first global mode, indicating that no fundamental modes exist below the frequency band of interest. The full diagonal elements of the upper residual matrix ***UR*** and the lower residual matrix ***LR*** are determined by solving a linear least-squares problem described by a reciprocal SISO modal model based on Eq. (2) and incorporating the reciprocity property expressed in Eq. (3). In this set of equations, involving only co-located DoFs %, the only unknows are the corresponding lower and upper residuals: LR_{oo} and UR_{oo}.

This estimated and expanded modal model is designed to capture both global and local flexability. It incorporates not only the contributions from the global fundamental flexible modes (the modal kernel term) but also those from the higher-fiequency truncated modes. These higher-fiequency modes play a crucial role in conecting local stiffness for all measured coupling degrees of freedom (DoFs).

Analysis & Results: Simulation Data

In this section, the workflow mentioned above will be validated using a dataset consisting of Frequency Response Functions (FRFs) extracted from a finite element model (FEM) of an EV battery, which contains 927712 nodes (see Fig. 4, left). The FRFs were simulated at 26 body-to-battery connection points, each with 3 tanslational degrees of freedom (DoFs) in the x, y, and z directions, resulting in a square FRF matrix with 78 rows (outputs) and 78 columns (inputs) at each frequency line. Figure 4, right, illustrates some typical FRFs simulated by the battery FEM. In our analysis, the frequency range was limited to $25 - 160$ Hz, as the FEM had been experimentally calibrated only up to this fiequency at the time of writing this paper. According to the FEM, the battery structure is expected to exhibit approximately 114 flexable modes within the $25 - 160$ Hz frequency range. Starting from the $78\,(N_o) \times 78\,(N_l)$ FRFs matrix extracted from the battery model, the goal is to identify a modal model that captures both the global flexible modes and the local flexability at the connection DoFs in this frequency band. The identification of that modal model must ensure both accuracy and relatively fast computation. The challenges arise from two main factors: 1) the number of flexable modes should be minimized while maintaining a good fit, and 2) local flexibility must be included for all the coupling degrees of freedom (DoFs) and this requires including all 78 columns of the FRFs matrix in the modal fitting process, which is computationally impractical.

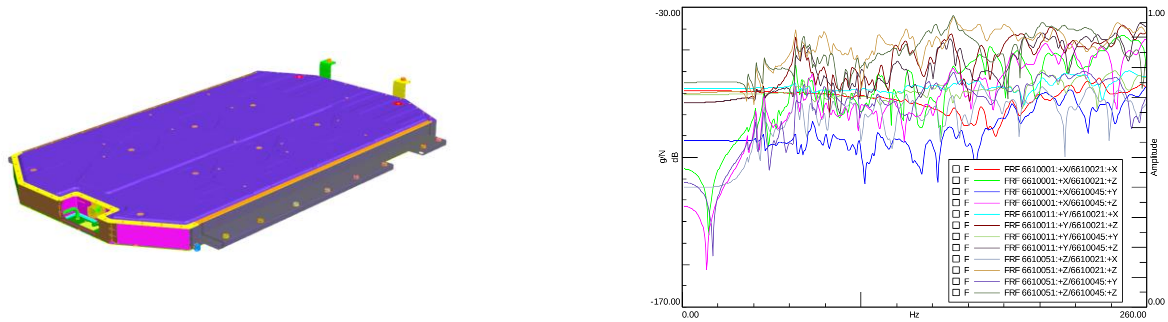

Fig. 4 The battery pack FEM (left) and some typical FRFs at connection points (right)

As mentioned in the workflow description section, the first step is to select a few columns from the full-size FRFs matrix, which originally contains 78 columns. By reducing the number of columns, the goal is to significantly speed up the modal estimation process of the global flexible modes. Four columns are selected, two conesponding to each of the two excitation locations shown in Fig 2-left (two columns per location). This results in a 78×4 FRFs matrix at each frequency line, which is then processed through the implemented FRFs balancing technique to equalize the magnitude levels of the 312 FRFs considered.

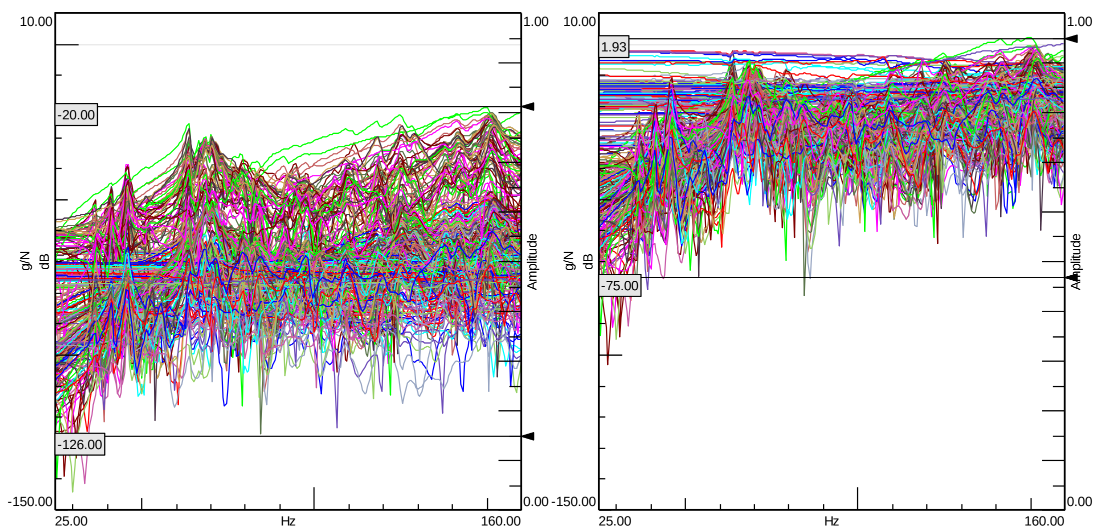

Fig. 5 Unbalanced FRFs matrix (left) & Balanced FRFs matrix (right)

Figure 5 shows the FRFs before and after applying the balancing technique. The balanced FRFs are visibly closer to each other in terms of their magnitude level compared to the unbalanced ones. This is also objectively reflected in the reduced dynamic range of the FRFs matrix after balancing, as shown in the figure.

Having balanced the FRFs matrix, the MLMM modal parameter estimator is then applied to the balanced matrix to optimize the modal model represented by Eq. (1) imposing the FRFs reciprocity, real mode shapes, and the negative mass sensitivity (NMS) constaints on the identified model. The MLMM optimization process is set to rum for 20 iterations, as convergence in the cost function evolution, as shown in Fig. 7, is observed starting from iteration 15. To start the iterations of the nonlinear optimization process in the MLMM estimator, reasonable initial values for the pole and the participation factors vector (i.e., λ_r, L_r parameters in Eq. (1) for each identified mode are needed. To estimate these initial values, the Polymax estimator, with a model size of 64, is applied to the balanced FRFs matrix. The Polymax-constructed stabilization chart is shown in Fig. 6, from which 48 modes are selected using the automatic modal parameter selection option [5]. The MLMM estimator then optimizes the initial values of the modal parameters of those 48 modes by minimizing the enror between the modal model (1) and the true (or the reference) FRFs. To evaluate the effectiveness of the FRFs balancing technique, the modal parameter estimation process, consisting of Polymax followed by 20 ML MM iterations, was conducted twice: first using the unbalanced (raw) FRFs matrix, and then using the balanced FRFs matrix.

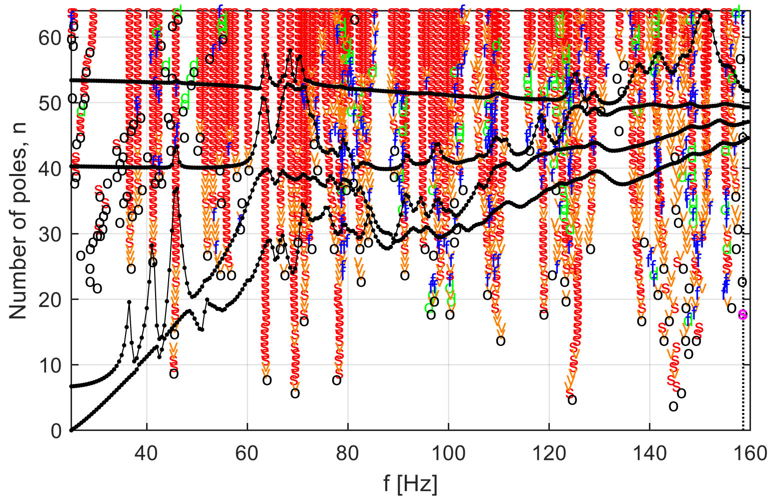

Fig. 6 Polymax stabilization chart (the black curves represent the 4 Complex Mode Indicator Function CMIIFs)

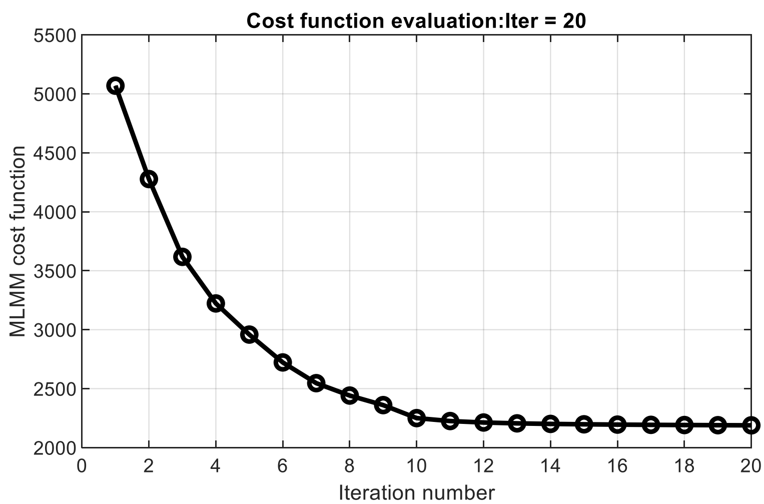

Fig. 7 MLMM iterations (the enror between the modal model and the true FRFs is decreasing over the different MLMM iterations)

Figure 8 shows color maps representing the relative modal synthesis enror percentage for each FRF, comparing two cases: with and without balancing the raw FRFs matrix before doing the modal estimation step. The relative modal synthesis enor is calculated as the sum of the errors between the reference FRF and the synthesized FRF across all frequency lines, divided by the reference FRF. As seen in these color maps in Fig. 8, balancing the FRFs matrix before performing modal parameter estimation improves the quality of the resulting modal model. This is evident from the lower relative modal synthesis enror percentage when using a balanced FRFs matnix compared to an imbalanced one. The improvement is particularly noticeable for FRFs with lower magnitude levels, such as those conesponding to excitation in the x and y directions. The modal synthesis of selected FRFs is presented in Figs. 9 and 10. Figure 9 illustates the modal synthesis for FRFs that originally have a low magnitude, while Fig. 10 shows the synthesis for FRFs with a higher magnitude. The results clearly demonstrate that balancing the FRFs matrix before performing modal parameter estimation improves the synthesis for lowmagnitude FRFs, without negatively affecting the synthesis for high-magnitude FRFs. Figure 11 displays the mode shapes of some extracted global flexible modes.

Once the reduced-size (78×4) reciprocal modal model is identified, the paticipation factor vectors, along with the diagonals of the lower and upper residual matrices, are extended using the expansion approach described earlier in the paper. This results in the final modal model which matches the size of the original full-size 78×78 FRFs matrix. Figure 12 judges

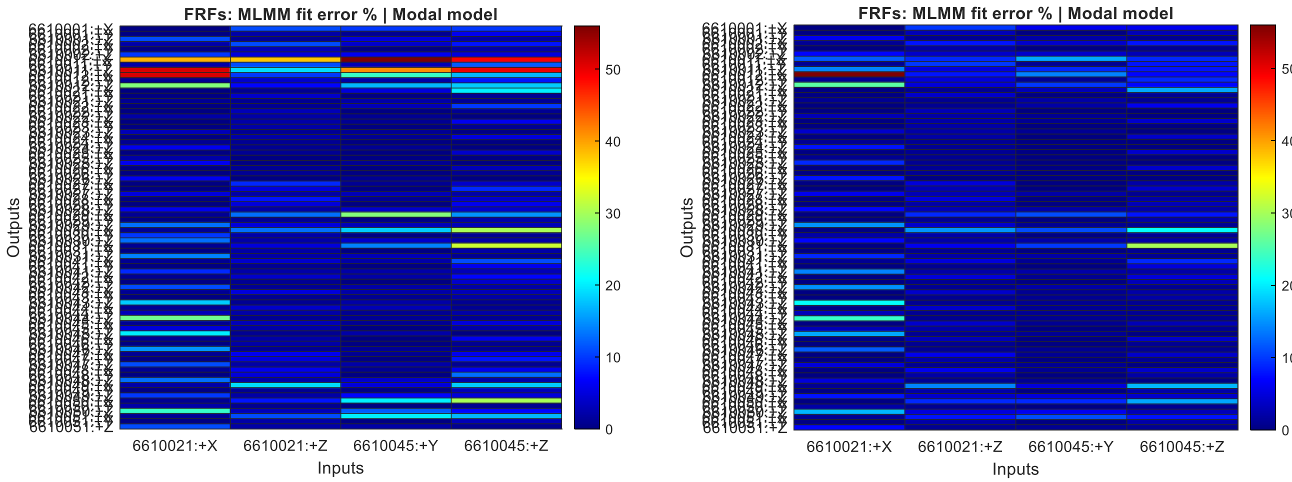

Fig. 8 The modal synthesis error % between the synthesized FRFs and the true ones without balancing the FRFs matrix (left) and with balancing the FRFs matrix (right)

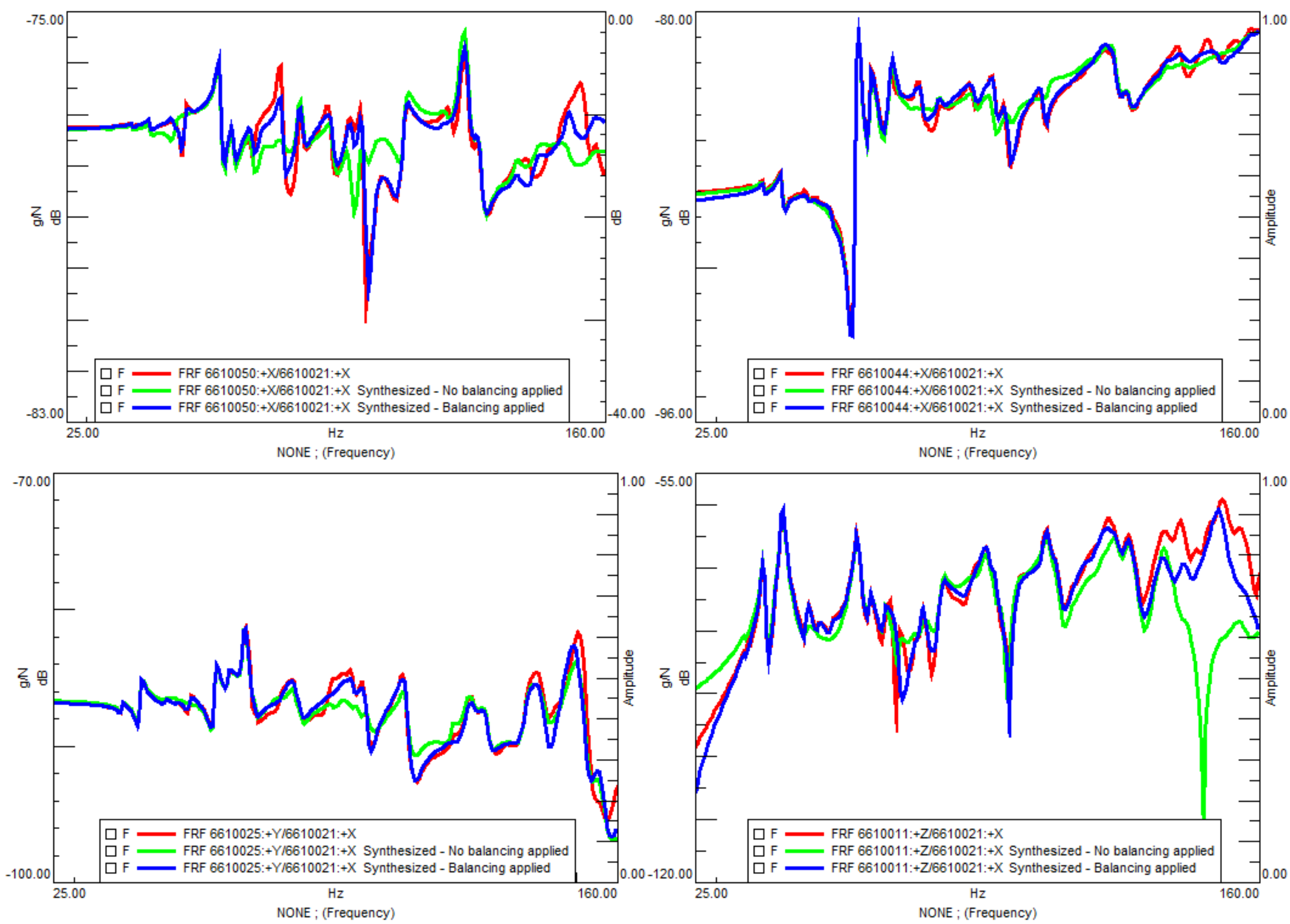

Fig. 9 The effect of the balancing approach on the quality of the final modal synthesis for some FRFs that originally have a low magnitude level

the accuracy of the expanded modal model by examining the modal synthesis of the FRFs of one driving point (in x, y, and z-directions) that were not initially included in the reduced-size FRFs matrix used to perform the modal parameter estimation. The figure illustrates the modal synthesis using three different approaches: 1) Modal estimation is performed directly with

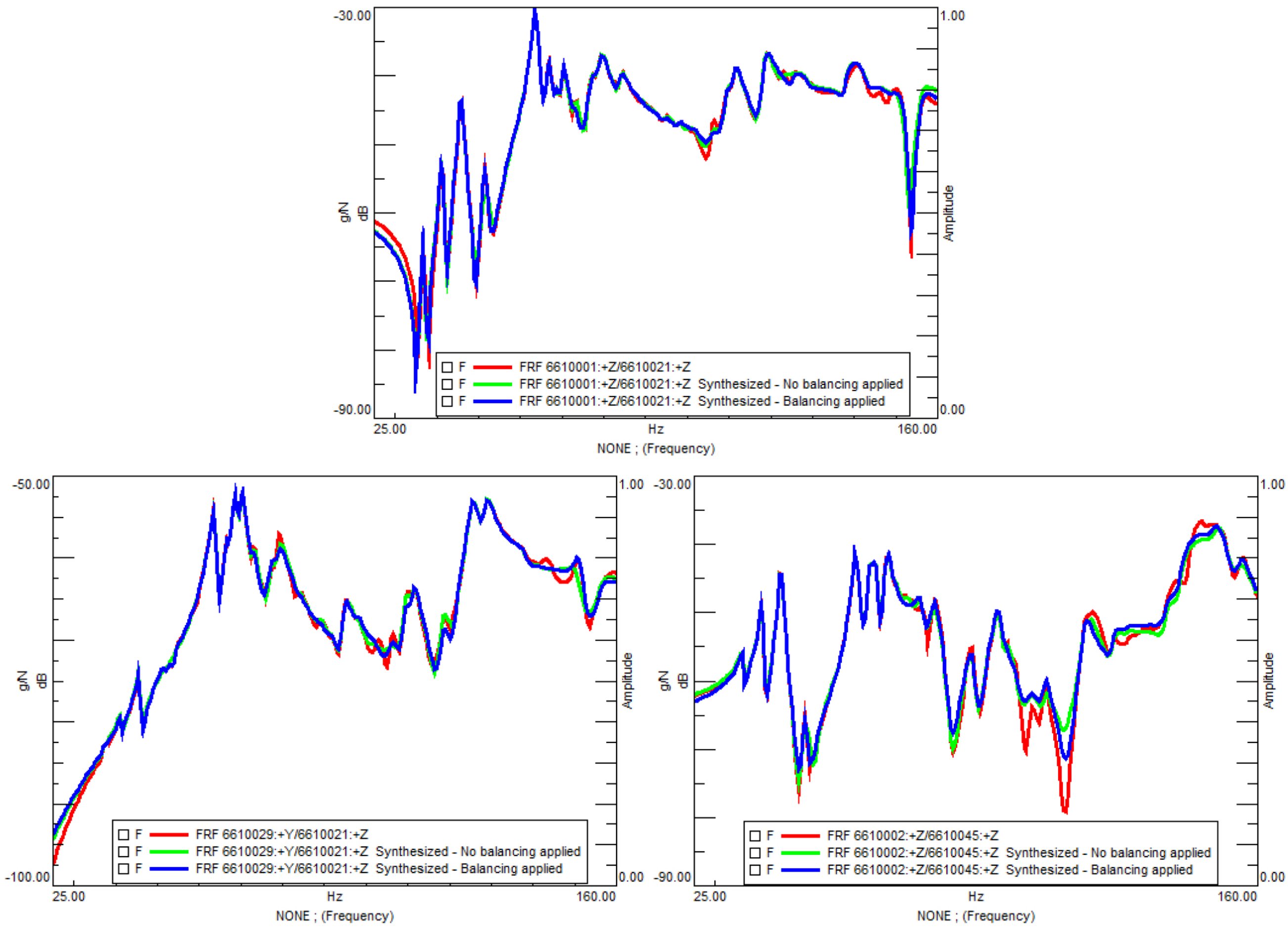

Fig. 10 The effect of the balancing approach on the quality of the final modal synthesis for some FRFs that originally have a high magnitude level

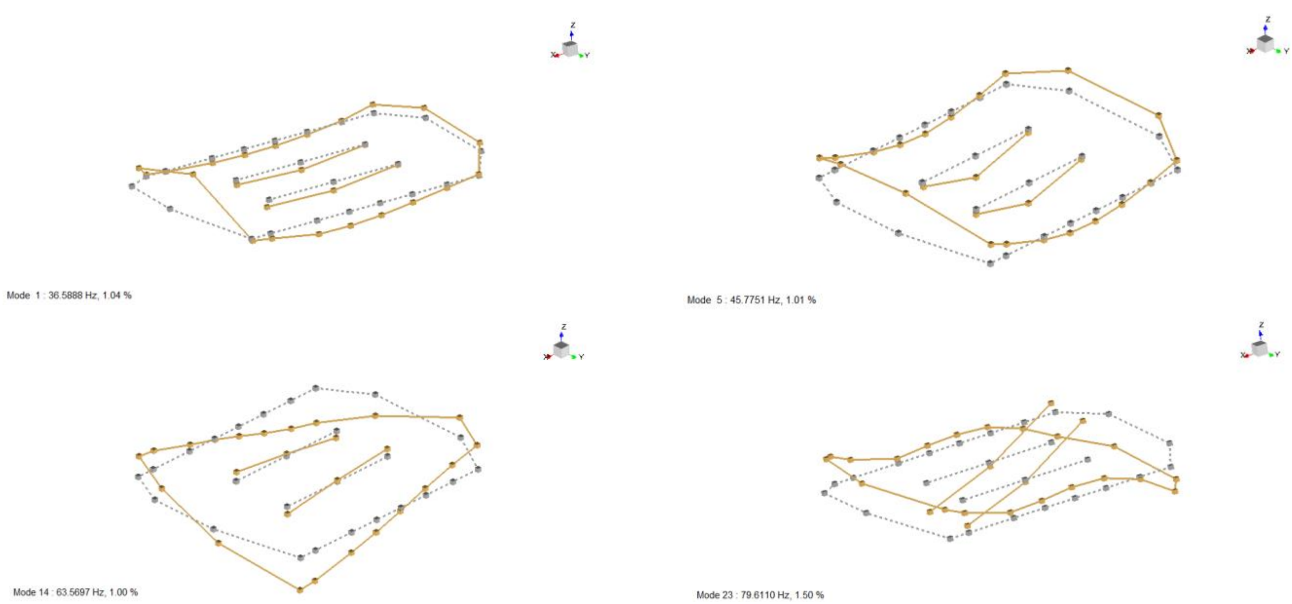

Fig. 11 Examples of estimated global flexible mode shapes

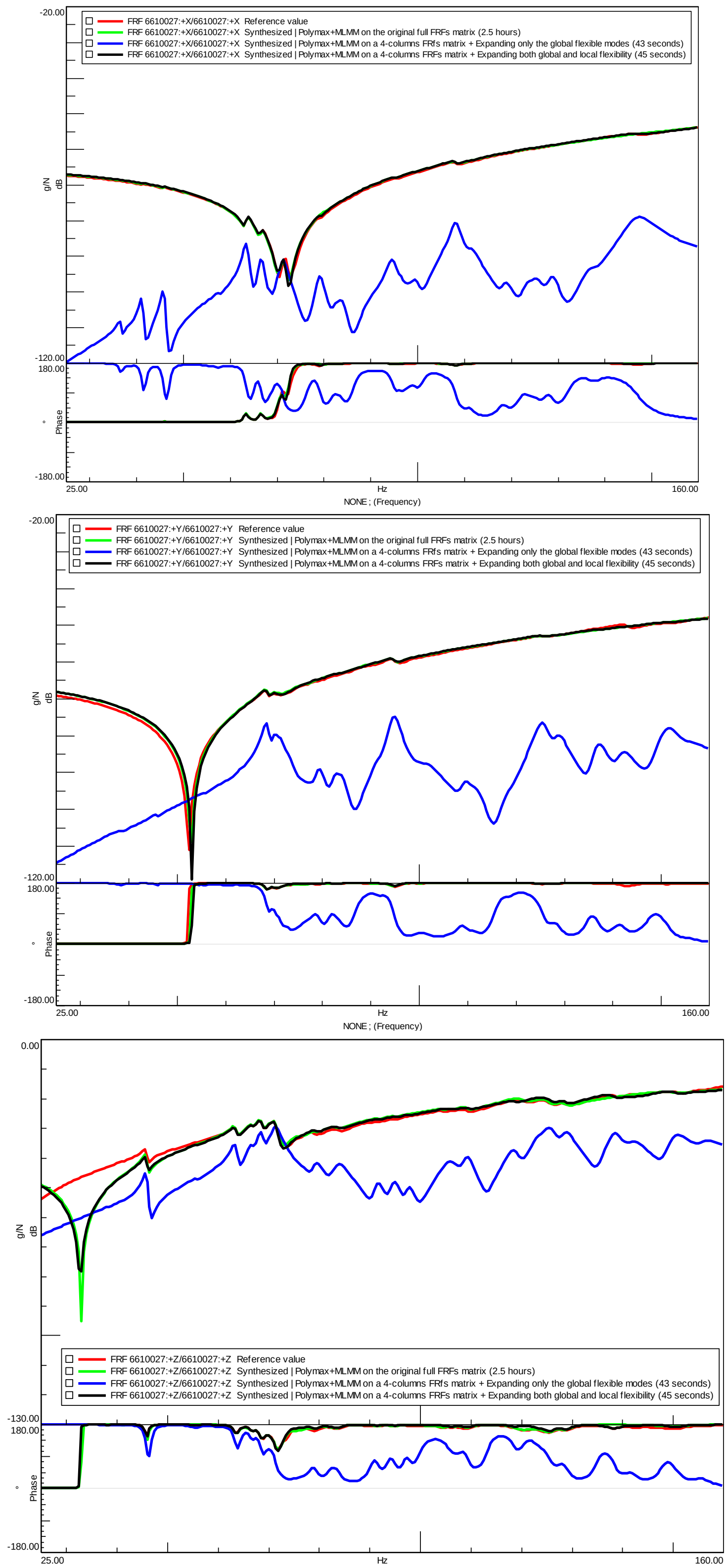

Fig. 12 The modal synthesis of FRFs of a connection point (in x, y, and z-directions) obtained from 3 different approaches for each the computational time is indicated in the figure legend (the shown FRFs were initially not included in the rechuced-size FRFs matrix that was used to perform the modal parameter estimation of the global flexable modes)

the full-size FRFs matrix (78 × 78), requiring no expansion; 2) Modal estimation is conducted with a reducedsize FRFs matrix (78 × 4), where only the contributions of global flexible modes are expanded while ignoring local flexibilities (i.e., the diagonal elements of the UR matrix); and 3) Modal estimation is carried out with the same reduced-size FRFs matrix (78 × 4), expanding contributions from both global and local flexibilities. The computational time for each approach is provided in the figure legend. The results from approach 2 in the Fig. 12 clearly demonstrate the importance of including local flexabilities. Ignoring this contribution leads to a significant degradation in the modal synthesis of the final identified modal model. Approach 1, which uses the full FRFs matrix, produces a modal model that closely fits the true FRFs. However, the computational time required for this approach is substantial (2.5 hours), making it impractical, especially for applications in vehicle design development. The lengthy computation time for approach 1 arises from the large mumber of parameters (27240) that must be optimized simultaneously during the MLMM iterations.

Figure 12 shows that approach 3 outperforms both approach 1 and approach 2 in terms of computational time and accuracy of the modal synthesis. Approach 3 delivers an accurate full-size modal model that accounts for both global and local flexibilities in just 45 seconds, significantly outperforming the other two approaches. This efficiency is evident from the quality of the modal synthesis achieved in a relatively short computational time. The reduced computational time of approach 3 is due to the optimization of only 8592 parameters, a significantly smaller number compared to the 27240 parameters in approach 1 , resulting in a more efficient process.

As a final validation step in this section, Fig. 13 illustrates the body-to-battery coupling results for a selected target DoF FRFs when the MLMM-based identified battery modal model, considering only 48 global flexible modes, is coupled to the vehicle body modal model (referred to as Assembly 2 in Fig. 13). These results are compared to the reference case modal system assembly (Assembly 1 in Fig. 13), which utilizes the full mode set identified by FEM for both the body and battery within the frequency band of interest. This full mode set includes 1,032 global flexible modes for the vehicle body and 114 for the battery, along with rigid body modes and static compensation modes to account for the truncated higher-frequency modes, as shown in Fig. 13. It is worth to mention that the Assembly 1 results were compared against a full body FEbattery FE assembly and the results were identical. Two key conclusions can be drawn from the results. First, the figure clearly demonstrates that the battery significantly impacts the NVH characteristics of the vehicle body. The system represented by the green curve (BIP - no battery coupled) exhibits a notably different response compared to the system represented by the red curve (battery coupled to the body with the full mode set). This highlights the importance of considering body-to-battery coupling when assessing the NVH performance of an electric vehicle (EV). Second, the coupling result obtained using the MLMM-based reduced-order modal model, considering both global and local flexibilities, albeit with only 48 flexible modes, closely matches the result from the full system assembly (Assembly 1, which includes 114 flexible modes for the battery). These findings validate that the proposed workflow effectively delivers a reduced-order modal model capable of adequately capturing the contributions of both global flexible modes and local flexibilities at the coupling degrees of freedom (DoFs).

Analysis & Results: Experdmental Data

In this section, the developed workflow will be tested and validated using test data that were measured churing a modal test of the battery structure. In this modal test, the battery structure was free-fiee suspended in bungees (cf. Fig. 14) and excited up to 2 kHz at 78 coupling DoFs (26 body connection points in x, y and z-directions) using the Simcenter Qsources hardware integral shakers (Qish-Integral shaker) mounted on Qtax excitation adaptor. Frequency response functions were measured consecutively under different multiple angles as shown in Fig. 14. The angled FRF set is processed to reconstruct the FRFs with the orthogonal imputs of the global axis system. The acceleration responses were simultaneously acquired at the 78 coupling DoFs using modal accelerometers PCB 356A15. This results in a $78\,(N_0) \times 78\,(N_0)$ FRFs matrix at each frequency line in the excited frequency range. Some typical measured FRFs are shown in Fig. 14.

In our analysis, we have targeted our fiequency application range $[100 - 1000$ Hz$]$ to start from the validated FB battery upper frequency limit ($<$ 160 Hz) and go up to the mid frequency range (1 kHz) where CAE body models can still be represented by FEM. A reduced FRF matrix consisting of only four columns is selected from the full FRF matrix to perform the modal estimation of the global flexible modes within the frequency band of interest more efficiently. Before applying the Polymax and MLMM modal parameter estimators to the reduced FRF matrix, the matrix is first balanced using the implemented balancing technique. The effect of the balancing process on the magnitude levels of the vanious FRFs is shown in Fig. 15. It can be observed that the FRFs get closer to each other in terms of magnitude after balancing. Figure 15 (bottom) provides a zoomed-in view of several FRFs with different magnitude levels. It is evident that after applying the balancing technique, the lower magnitude FRFs increase in magnitude, becoming closer to those with higher initial magnitudes.

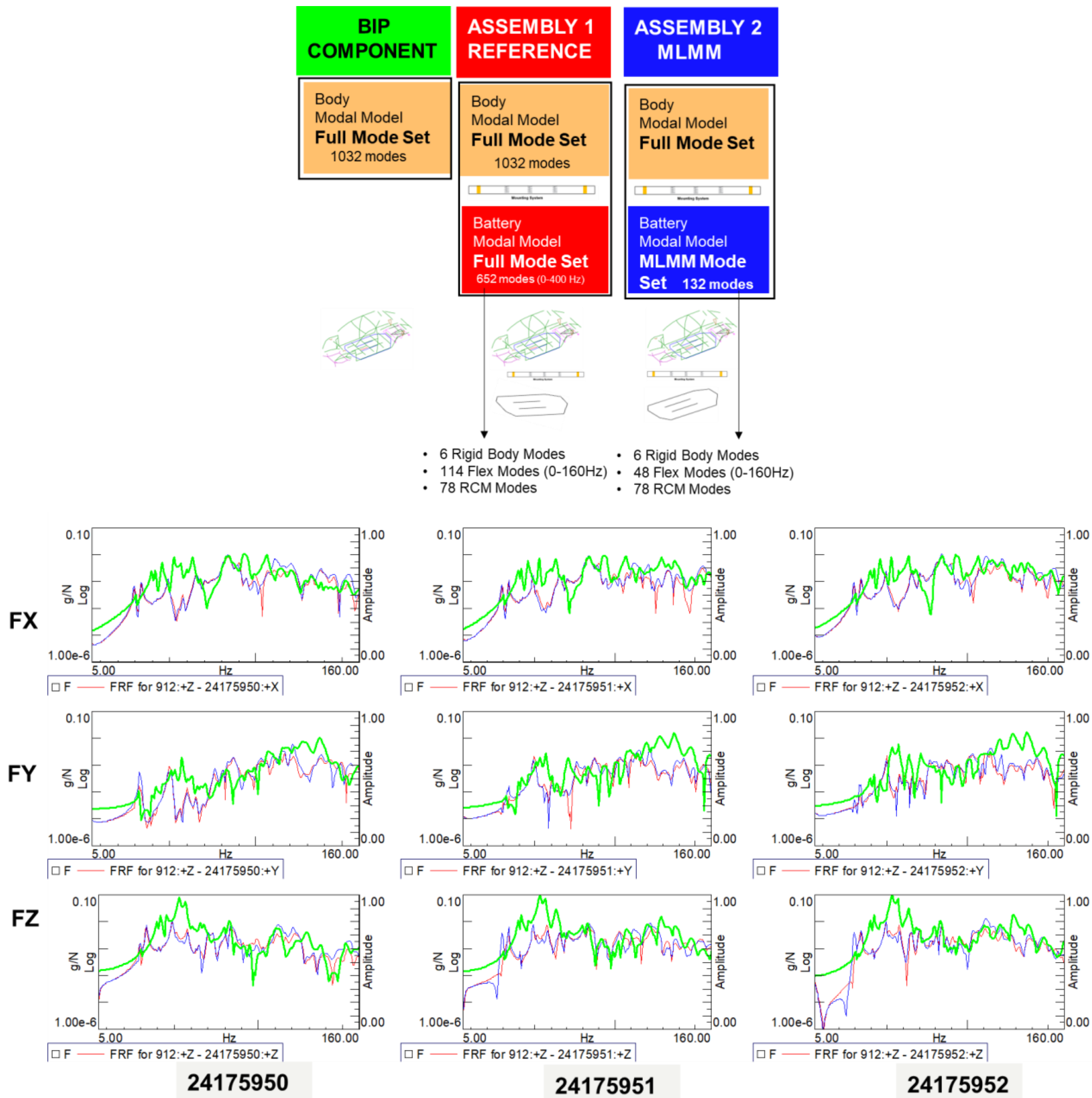

Fig. 13 Body-to-battery coupling results — Reference assembly versus the MLMM-based modal system assembly — The shown result is for the seat rail vibration as a body target response (912:+Z) and unit body load at the rear engine mount locations (24175950,24175951,24175952 +X, +Y, and +Z)

The Polymax estimator with a modal size of 200 is then applied to the balanced reduced-size FRF matrix to estimate the initial modal model, which will be used to initiate the MLMM optimization iterations. Figure 16 presents the clear stabilization diagram constructed by the Simcenter Polymax estimator, from which 47 modes were manually selected with the aid of the four Complex Mode Indicator Functions (CMIF) overlaid on the same figure. Stating with the Polymax-based initial modal model, the MLMM estimator was run for 30 iterations, imposing constraints, i.e., reciprocity, real mode shapes, and negative mass sensitivity, on the optimized modal model Fig. 17 illustrates the different iterations of the MLMM optimization process, showing a gradual decrease in the fit error over the iterations. For companison, the modal estimation process was also conducted using the imbalanced (raw) FRFs with the same user settings. Once the modal parameters are estimated they are rescaled back to make them consistent with the original magnitude level of the raw FRFs.

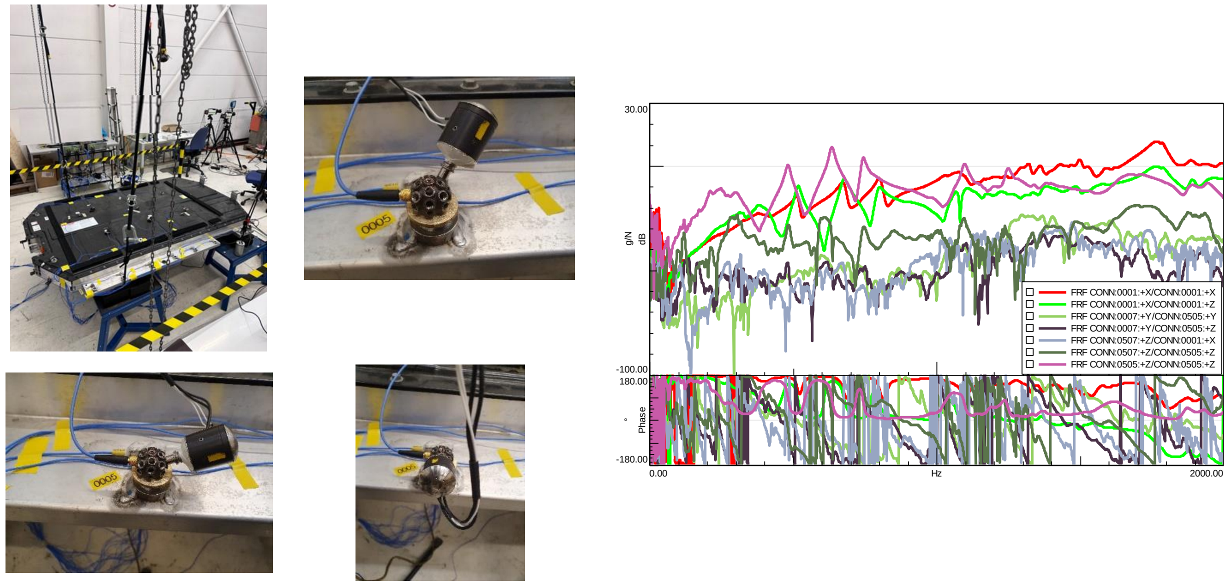

Fig. 14 The battery test set-up and some typical measured FRFs at comection points

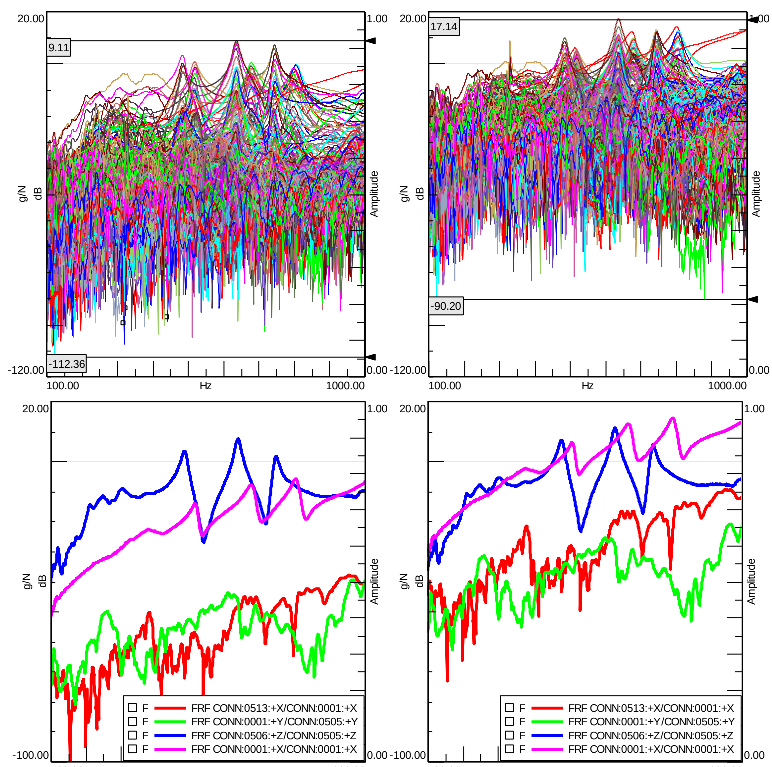

Fig. 15 The effect of the implemented FRFs balancing approach on the magnitude level of the measured FRFs (Top: all the FRFs, Bottom: zoom-in on a few FRFs, Left: imbalanced (raw) FRFs, and Right: balanced FRFs

In Fig. 18, it can be observed that for FRFs with lower initial magnitudes, the final retrieved modal synthesis is improved when the FRF matrix is balanced before performing the modal parameter estimation (see Fig. 18 - bottom). For FRFs with higher initial magnitudes (see Fig. 18 - top), the solution based on the balanced FRFs is similar to that from the raw FRFs, indicating that applying the balancing technique does not negatively affect the quality of the modal synthesis for FRFs

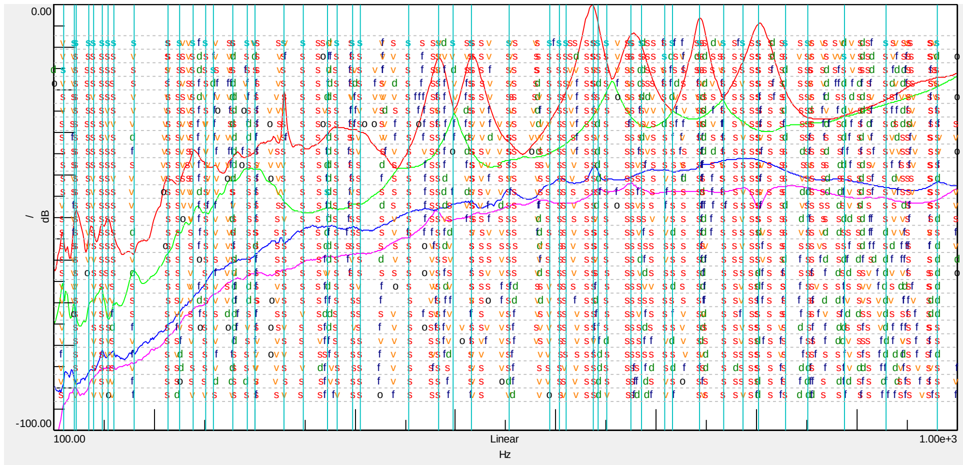

Fig. 16 Polymax stabilization chart when applied to a battery measured FRFs with 4-references (the shown curves represent the 4 Complex Mode Indicator Function CMIFs)

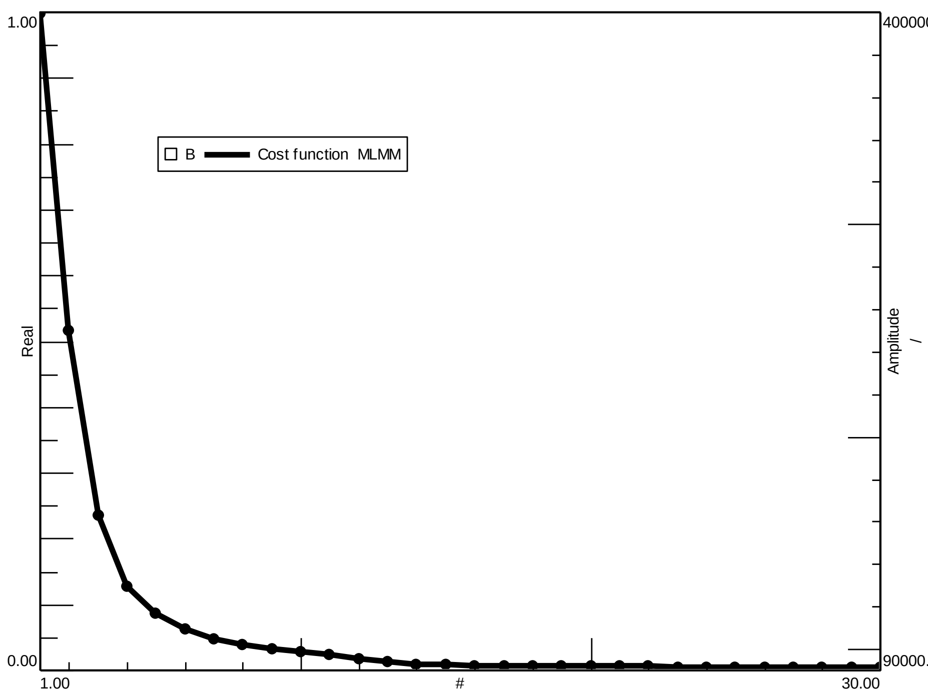

Fig. 17 The MLMM iterations to optimize a test-based battery modal model (the enror between the modal model and the true FRFs is decreasing over the different MLMM iterations)

with higher initial magnitudes. The auto-MAC of the estimated mode shapes from the two considered cases (i.e., with and without balancing the FRF matrix) is shown in Fig. 19. It is clear from the figure that using a balanced FRF matrix results in a less correlated set of mode shapes compared to the case where an unbalanced FRF matrix is used. In the final step, the reducedsize (78×4) modal model is expanded to the full size of the measured FRF matrix (78×78) by filling in the missing elements of the participation factor vectors and the diagonals of the residual term matrices. The missing participation factors for each mode are calculated using the estimated reciprocal scaling factor, thanks to the reciprocity constraint imposed in the MLMM optimization

The missing diagonal elements of the lower and upper residual term matrices are found by fitting the obtained expanded reciprocal modal model in a SISO fashion to the conesponding driving point FRF, where all the modal parameters of the

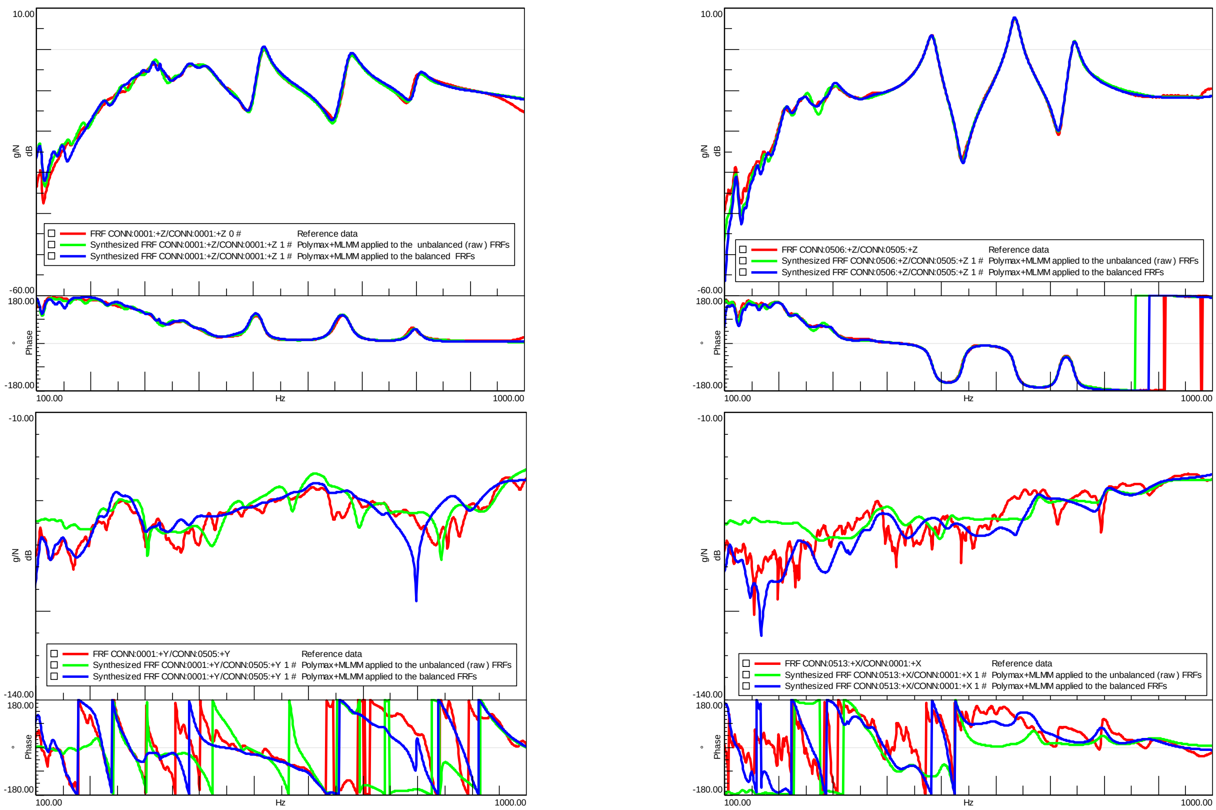

Fig. 18 Modal synthesis of the test-based MLMM estimated battery modal model (Top: FRFs with higher initial magnitudes & Bottom: FRFs with lower initial magnitudes)

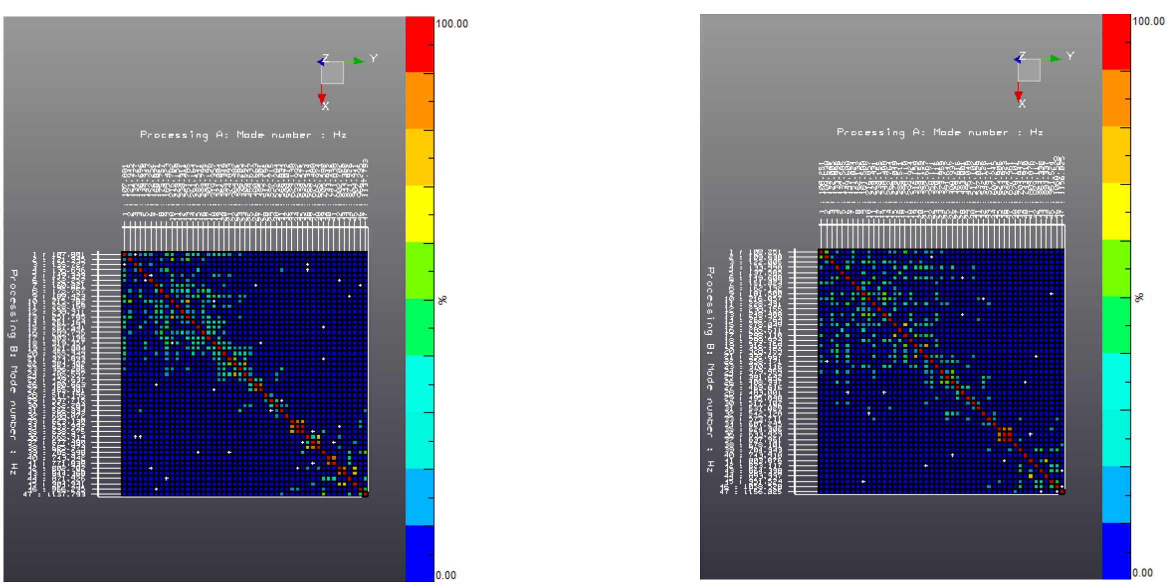

Fig. 19 The Auto-MAC function of the estimated mode shapes — Left: Estimated based on the unbalanced (raw) FRFs & Right: Estimated based on the balanced FRFs

global flexible modes are already known, and only the UR and LR terms remain as unknowns. The results of the expansion process are shown in Figs. 20 and 21, focusing on modal synthesis accuracy. In Fig. 20, the modal fit enor percentage, calculated between the measured and synthesized FRFs, is shown for both the initially considered 4 columns and the expanded

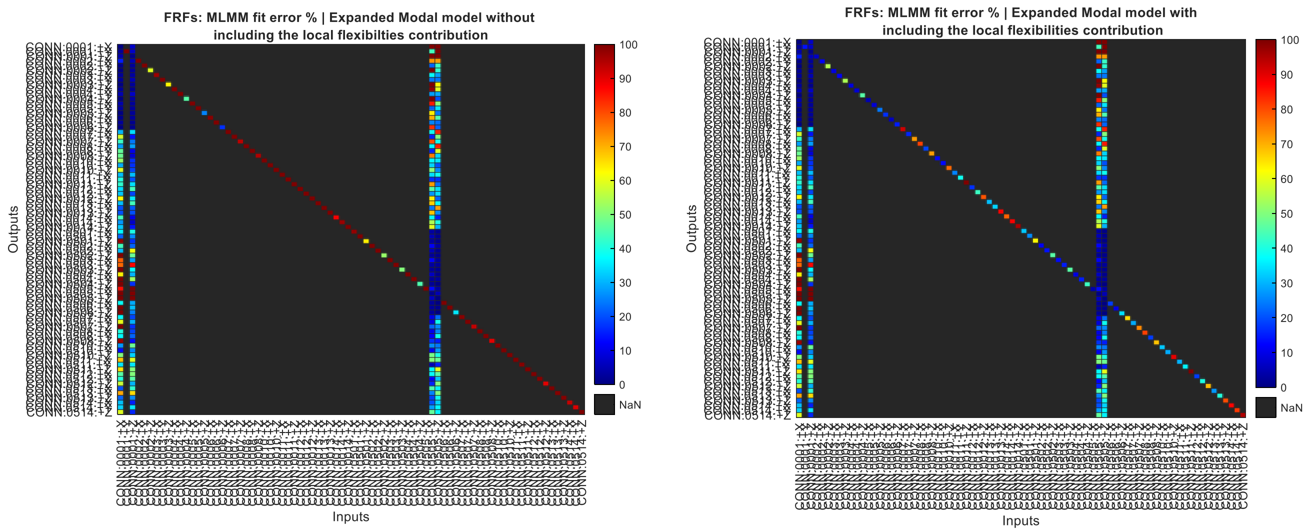

Fig. 20 Modal synthesis error $\%$ of the expanded modal model without and with including the local flexabilities contribution in the expansion (ie. upper residual term for the expanded driving points FRFs)

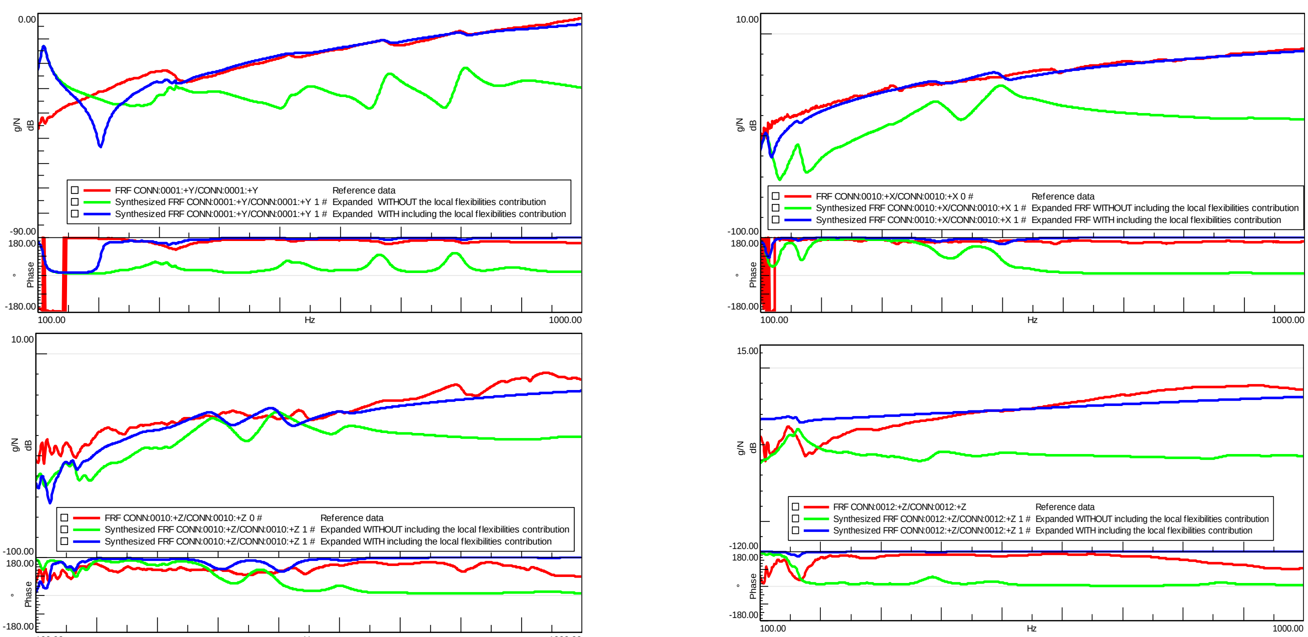

Fig. 21 Modal synthesis for driving points FRFs that were not included in the modal estimation step (i.e., FRFs calculated from the modal model expansion process)

driving point FRFs (i.e., those not included in the modal estimation step). Figure 21 illustrates the modal synthesis over the frequency band of interest for some selected expanded driving point FRFs. In general, one can see that the expansion process delivers a reasonable modal synthesis for most of the driving point FRFs that were originally not considered in the modal estimation step. The key takeaway from these figures is that expanding only the contributions of the global flexable modes is insufficient to achieve accurate synthesis for a driving point FRF that was not originally included in the modal estimation step. The inclusion of residual effects, which compensate for the trumcation of higher-frequency modes (i.e, local flexibilities), is essential for achieving an accurate modal synthesis of such an FRF.

From the presented results in this section, it can be seen that the proposed 2 -step modal parameter estimation workflow is successful in delivering a full-size modal model, acceptable in accuracy and compact in size, which considers both global flexible modes that are in within the frequency-band of interest together with the trumcated higher frequency modes' residual effects at all the considered DoFs. Key in the developed workflow is that it can be executed in a timely efficient way starting from only a reduced set of FRFs. Futhermore, the resulting modal model is directly suitable to be coupled as a modal superelement in a full vehicle (FV) Nastran model. Subsequent FV response analysis can be run efficiently in SOL111 without any frequency-dependent stiffness properties, umlike FRF-based substructuring methods.

Conclusion

In this paper, we introduced and validated an enhanced modal parameter estimation workflow aimed at improving the accuracy and efficiency of the NVH performance characterization process for electric vehicles, particularly in handling the challenges posed by large-scale unbalanced frequency response function (FRF) datasets. The workflow, leveraging the MLMM modal parameter estimator, demonstrated effectiveness in addressing common issues such as magnitude imbalances in FRF data and computational inefficiencies when dealing with a FRFs matrix with a large number of columns. Key contributions include the implementation of a magnitude-based FRF balancing technique and an expansion approach to enhance both global and local modal characteristics of the structure under test are introduced in this work. The presented magnitude-based balancing technique was proved to improve the final modal synthesis of those FRFs that come with lower initial magnitudes while not negatively affecting those which come with higher initial magnitudes. The introduced modal expansion approach helped to deliver an acceptable accurate modal model that considers the contributions of both global flexible modes and local flexibilities at all the considered DoFs in an efficient way. The findings highlight the importance of considering both global flexible modes and local flexibilities in order to have an accurate modal synthesis for all the considered DoFs, and this becomes more significant for the DoF that corresponds to a driving point. The validation, both through simulation and experimental data, confirmed that the developed workflow can efficiently handle complex fiequency response functions (FRFs) matrices, significantly reducing computational time while maintaining a reasonable accuracy in modal synthesis. Finally, the developed workflow is fit for integration in a full vehicle development process, combining seamlessly test and FE based components.

Acknowledgments The authors gratefully acknowledge the support of VLAIO (Flemish Innovation & Entrepreneurship) through the O&O project ADRENALINE (HBC.2022.1027). The authors gratefully acknowledge the support of Hyundai Motor Company (HMC) both for providing the battery hardware and the FB model.

References

1. Klerk, D. D., Rixen, D. J., & Voonmeeren, S. N. (2008). General Framework for Dynamic Substructuring: History, Review and Classification of Techniques. AIAA Joumal, 46(5), 1169-1181. doi:10.2514/1.33274
2. Peeters, B., Van der Auweraer, H., Guillaume, P., and Leuridan, J., The PolyMAX frequency-domain method: a new standard for modal parameter estimation, Shock and Vibration, vol. 11, pp. 395-409, 2004.
3. Elkafafy, M, Peeters, B., Guillaume, P., and De Troyer, T., Constrained maximum likelhood modal parameter identification applied to structural dynamics, Mechanical Systems and Signal Processing, vol. 72-73, pp. 567-589, 2016.
4. Heylen, W., Lammens, S., Sas, P., Modal Analysis Theory and Testing, Heverlee: Katholieke Universiteit Leuven, Department Werktuigkunde. 2016.
5. Lanslots, J., Rodiers, B., Peeters, B., Automated pole-selection: proof-of-concept & validation, In Proceeding of the ISMA2004 International Conference on Noise and Vibration Engineering, Leuven, Belgium, 2004.